Electrochemically grown vertically aligned ZnO nanorod array/p^+-Si (100) heterojunction contact diodes.

Jorge Rodríguez-Moreno[1], Elena Navarrete-Astorga[1], Rocio Romero[2], Francisco Martín[1], Ricardo Schrebler[3], José R. Ramos-Barrado[1], Enrique A. Dalchiele[4]

[1]*Laboratorio de Materiales y Superficies (Unidad Asociada al CSIC). Departamentos de Física Aplicada & Ing. Química, Universidad de Málaga, E29071 Málaga, Spain.*

[2]*Unidad de Nanotecnología, Edif. Bio-innovación y Nanotecnología, Universidad de Málaga, C/Severo Ochoa 34, Parque Tecnológico de Andalucía, Campanillas, 29590 Málaga, Spain.*

[3]*Instituto de Química, Facultad de Ciencias, Pontificia Universidad Católica de Valparaíso, Casilla 4059, Valparaíso, Chile.*

[4]*Instituto de Física, Facultad de Ingeniería, Herrera y Reissig 565, C.C. 30, 11000 Montevideo, Uruguay.*

Number of pages:	*25, including title page, abstract, main text, references and figure captions.*
Number of tables:	*0*
Number of figures:	*5*
Running title:	*"ZnO-nanorods-p-type-silicon-diode"*

Please address correspondence related to this paper to: Enrique A. Dalchiele, dalchiel@fing.edu.uy , Tel. ++598-2-7110905, Montevideo, Uruguay.

Abstract. ZnO nanorod array/p^+-Si vertical heterojunction diodes, in which the ZnO nanorods have been grown by electrodeposition onto a FTO/glass substrate, have been fabricated by the direct-bonding technique. The heterojunction diode device showed a very good rectifying behavior with a rectification ratio of the forward-to-reverse bias current as ca. $2.5x10^4$ at a voltage of ±10 V. The I-V characteristic was examined in the framework of the thermionic emission model. The obtained ideality factor and the barrier height values of the diode are 2.8 and 0.85 eV, respectively. The conduction mechanisms have been investigated from I-V characteristics as well.

Keywords: ZnO nanorod arrays, p-type silicon, heterojunction diode, electrodeposition.

1. INTRODUCTION

Zinc oxide (ZnO), a direct wide bandgap semiconductor (Eg=3.37 eV), is considered a promising electronic material for optoelectronic devices, solar cells and for the next generation of UV light emitting diodes because it has a large exciton binding energy (~60 meV), which allows efficient excitonic emission at room temperature [1-3]. Moreover, its nanostructures have attracted great attention as a promising functional material. Among the various ZnO nanostructures, well-aligned nanorod (NR) and nanowire arrays have been extensively explored due to their good physical properties [4-8]. In fact, these structures have high aspect ratio and a high surface area, and can provide a direct conduction path for electrons [5]. The charge carrier transport and collection in nanowires is expected to be improved with respect to the two dimensional planar layer owing to their very high crystalline quality [9]. In addition, ZnO nanowires have excellent electron transport capabilities resulting from internal electrical fields in the direction of the c-axis of wurtzite crystals [5]. ZnO with a wurzite structure is naturally an n-type semiconductor because deviation from stoichiometry due to the presence of intrinsic defects such as oxygen vacancies (V_O) and zinc interstitials (Zn_i) [10]. Consequently, as-grown ZnO exhibits always an n-type electrical conductivity, due to these native defects. On the other hand, a reproducible method to grow p-type ZnO films and nanostructures, necessary for fabrication of ZnO p-n homojunctions, is still a challenge due to several reasons such as deep acceptor levels, low solubility of the dopants, and the self-compensation process [4,11-13]. So, for the moment, reproducible and stable p-type ZnO material with sufficiently high conductivity and carrier concentration is still in a development phase. Though some ZnO-based homojunction diodes and LEDs have been reported in the literature [4], the optoelectronic performances of those devices are still relatively poor and the time-dependent reliability

in air is controversial due to the strong self-compensation effect of p-ZnO [4,12]. For that reason, instead of ZnO-based homojunction devices, a number of works have been focused on the fabrication of heterojunction devices, by replacing p-type ZnO with other p-type inorganic (p-Si, p-GaN, p-NiO, p-SiC, p-Cu_2O) [11,14,15], or organic (poly(3,4-ethylenedioxythiophene (PEDOT), poly(3-hexylthiophene-2,5-diyl) (P3HT)) [16-18] materials. As silicon already has a vital position in the microelectronic industry, heterojunctions between Si and ZnO need to be investigated [19]. Most of the studied n-ZnO/p-Si heterojunctions are based in ZnO thin films [11,20-23]; there are only few reports on the n-ZnO NR arrays/p-Si heterojunction devices [15,19,24-26]. In a general way, those n-ZnO NR arrays/p-Si heterojunction diode structures have been prepared by growing the ZnO NR arrays onto p-Si substrates by different techniques (i.e.: vapor liquid solid [19], hydrothermal method [15], chemical vapor deposition [25], metalorganic chemical vapor deposition [26]), and afterwards the ohmic contacts have been done. In the last years, a different simple but feasible direct-bonding technique has been reported in diode and LED fabrications [12,27,28], in which n-ZnO NR arrays are first grown onto a foreign conductive substrate, and then the bonding heterojunctions can be easily formed by pressing the p-type semiconductor chip onto the tips of this ZnO NR arrays [12,27]. Then, p-n heterojunction structures and electrodes can be formed without using hard and complex procedures (i.e.: lithography and reactive ion etching), thus simplifying the device packaging [12]. In fact, by using this novel technique, very promising and encouraging results have been obtained in n-ZnO NR/p-GaN [12] and n-ZnO NR/p-Si [27] light-emitting diodes. In the last reported literature case, ZnO NR arrays have been fabricated by a vapor-phase transport technique [27], and in general the fabrication processes mostly involve relatively high temperature and high cost growth methods [25,26]. Therefore, in order to realize more extensive

applications of n-ZnO NR arrays based diodes and LEDs, low-temperature, low-cost and controllable processing procedure should be developed [14]. In this sense, electrochemical deposition has been proved to be a simple, low temperature, and cost-effective large-area deposition technique for thin films and nanostructured semiconductor materials [29-32]. As the electrochemical method would naturally provide a good electrical contact between NR arrays and the conductive substrate, hence offers a convenient starting point for a variety of interesting optoelectronic applications at the nanoscale level [33]. Moreover, electrochemical growth procedure produces highly crystalline (single crystalline) nanowires/nanorods of excellent electronic quality [6,7,34,35]. Related to zinc oxide material, electrodeposition allows an excellent control of ZnO nanostructure morphology and size (i.e.: aspect ratio). This could be achieved by playing on different deposition parameters such as: the precursor's concentration, the electrolytic bath temperature, the applied potential and the charge passed during electrodeposition [1,34].

In the present work, vertical heterojunction contact diodes composed of electrodeposited vertically aligned n-ZnO NR arrays and p^+-Si using the direct-bonding technique are fabricated and characterized. The as-grown ZnO NRs were investigated in terms of their morphological and structural properties. Moreover, the electrical performance of the resulting heterojunction diodes was systematically investigated through the current-voltage (I-V) measurements.

2. EXPERIMENTAL DETAILS

Synthesis of ZnO nanorod arrays.

ZnO nanorod arrays were grown by the electrochemical deposition method from a 0.5 mM zinc chloride aqueous solution maintained at 70 ^{o}C. For supporting electrolyte, 0.1 M potassium chloride was employed to ensure a good electrical conductivity in the aqueous solution (Milli-Q quality water, 18 MΩ.cm). The pH of the solution was initially adjusted to 6.8. The ZnO nanorods were grown onto transparent electrode substrates, consisting of glass plates with a conductive thin film of fluorine-doped tin oxide (SnO_2:F, FTO) on one side (Nippon Sheets, sheet resistance of about 10-30 Ω/□). The electrodeposition was performed in a conventional three-electrode electrochemical cell with the substrate as the cathode, a platinum sheet as the counter electrode and a saturated calomel electrode (SCE) as the reference one. Electrodeposition was carried out potentiostatically at -1.414 V vs. saturated mercury-mercurous sulfate reference electrode (SMSE) by using an Autolab PGSTAT30 potentiostat/galvanostat. The electrolyte was saturated with pure molecular oxygen by bubbling for 45 min prior to start the electrodeposition and continuously during of the growth process. The electrochemical deposition time was 7200 s. After electrodeposition, the ZnO NR arrays/FTO/glass substrate samples were thoroughly and carefully rinsed with DI water to remove un-reacted products from the surface and dried under a moderate air flux.

Morphological and structural characterization of ZnO nanorod arrays.

Field-emission scanning electron microscopy (FE-SEM) pictures of the ZnO NR arrays were obtained on a Helios Nanolab 650 Dual Beam from FEI company equipment.

Transmission electron microscopy (TEM), high transmission electron microscopy (HTEM), and selected area electron diffraction (SAED) have been carried out with a Philips CM-200 microscope operated at 200 kV. Specimens for TEM were prepared by removing the electrodeposited NR array by grating with a scalpel, collected and ultrasonically dispersed in 1 ml of ethanol. A small drop of the suspended solution was placed onto a porous carbon film supported on a TEM nickel grid, and was dried in air prior to observation.

Structural characterization of the ZnO nanorod arrays was examined by X-ray diffraction (XRD) by using a Philips X´Pert PRO MPD diffractometer at the low angle configuration using CuK_{α} radiation (with a Ge(220) hybrid primary monochromator). The accelerating voltage was set at 45 kV with a 35 mA flux. Measurements have been done at an omega angle of 0.8^{o}.

Fabrication of ZnO nanorod arrays/p^{+}-Si (100) heterojunction contact diodes.

A heavily B-doped p^{+}-Si (0.001-0-09 Ω.cm) wafer chip of 2x3.5 cm^2 in size was used as a hole injecting electrode. For device fabrication, the p-n heterojunction was formed by pressing the p^{+}-Si wafer chip vertically onto the top tips of the ZnO NR array on the FTO/glass substrate. The contact area of 1x2 cm^2 was pressed by 100 g weight and fixed using a transparent epoxy. Then, the device was post-thermally treated in a tube furnace at 150 ^{o}C for 1 h under air environment to improve the physical bonding at the p-n heterojunction interface. Ohmic contact to p+-Si(100) has been done, following previously reported works in the literature [36,37], by using Ga-In eutectic. The contact to ZnO NR array is directly provided by the FTO substrate, as the FTO/glass acts as the

substrate for the ZnO NR array (they have been electrochemically grown onto it), and as the conductive electrode that collect the current circulating through the circuit.

Electrical characterization of ZnO nanorod arrays/p^+-Si (100) heterojunction contact diodes.

An Autolab PGSTAT30 potentiostat/galvanostat was used to measure the I-V characteristics of the diode devices. All measurements were performed at room temperature and in dark conditions.

3. RESULTS AND DISCUSSION

Morphological and structural characterization of ZnO nanorod arrays.

Figure 1a shows typical FESEM micrograph of ZnO nanorod arrays electrochemically grown onto a FTO/glass substrate. It can be appreciated that all of them show hexagonal cross section and hexagonal faceted (which arises due to their wurtzite structure) [1,8] and exhibited planar top ends (see inset of Fig. 1a). Moreover, the majority of the nanopillars are mostly vertically oriented to the substrate plane and the axial direction is aligned with the c-axis of the hexagonal ZnO crystal structure. The nanorod mean diameter is in the range 70-140 nm with a length of about 1 μm, giving rise to nanorods with an aspect ratio of about 7-14. The single crystallinity of the ZnO nanorods is evident from their faceted crystal habit and from XRD results (vide infra), and confirmed by HRTEM analysis (vide infra). The detailed microstructure of the ZnO NR arrays is further investigated by transmission electron microscopy (TEM)-related

techniques. Figure 1b shows a TEM image of a typical ZnO NR physically removed from the FTO substrate, exhibiting a diameter of 120 nm, which also confirms that the diameter of the ZnO NR array is in the range of 70-140 nm. HRTEM image focused on the ZnO NR and the corresponding selected-area electron diffraction (SAED) pattern (Figures 1c and 1d) confirmed that it had a single crystal wurtzite structure and was grown along the c-axis direction with 0.26 nm (0002) lattice fringe parallel to the basal plane [38].

Figure 2 shows a typical X-ray diffraction pattern of a ZnO nanorod array sample as well as the standard reference powder diffraction pattern for hexagonal ZnO [38]. All the X-ray diffraction peaks can be indexed to the hexagonal wurtzite ZnO structure. No any other diffraction peaks besides SnO_2 which comes from the FTO/glass substrate were detected, indicating high purity of the hexagonal ZnO phase. The predominant ZnO (0002) diffraction peak is observed, revealing on one side that the ZnO nanorods are highly crystalline, and on the other side indicating they vertical growth along the vertical *c*-axis. This is in good agreement with the SEM views that show that the nanorods have a hexagonal section and with HRTEM results, presented above. The (0002) peak is very sharp with FHWM of 0.13^{o}. Three other diffraction peaks are present and correspond to the (10$\underline{1}$0), (10$\underline{1}$1) and (10$\underline{1}$3) planes of wurtzite ZnO. Their intensity is very low compared to the (0002) one.

Electrical properties of ZnO nanorod arrays/p^{+}-Si (100) heterojunction contact diodes.

Figure 3a shows schematic cross-section of the ZnO nanorod array/p^{+}-Si (100) heterojunction contact diode device. The electrochemically grown n-ZnO nanorod

arrays aligned vertically to the FTO/glass substrate in contact with the p^+-Si wafer chip form the point p-n heterojunctions. The junction properties were examined by current-voltage (I-V) measurements at room temperature in air under dark conditions. Prior to examining the rectifying properties of the heterojunction diode, it is necessary to confirm ohmic behaviors of the electrodes. Figure 3b shows the I-V characteristics of the FTO/ZnO NRs contact, and that for a device as in Fig. 3a but without the presence of the ZnO NRs (i.e.: FTO/glass substrate directly contacted to the p^+-Si(100) chip), thus simulating a possible short-circuit between FTO and p^+-Si(100) in the ZnO nanorod array/p^+-Si (100) heterojunction contact diode device. The I-V curves obtained from the FTO/p^+-Si(100) device (without the presence of ZnO NRs) and from contact FTO/ZnO exhibit a linear ohmic behavior and a slightly rectifying but symmetrical electrical behavior, respectively (see inset Fig. 3b).

A typical I-V characteristic curve of the obtained diodes is displayed in Fig. 3c. It can be clearly seen that the device exhibits good rectifying behavior, indicating the formation of a diode. This observed rectifying behavior is due to the n-p heterojunction ZnO NRs/p^+-Si(100) because contacts are either nearly ohmic or good ohmic, as described above. The device shows a low turn-on voltage (V_{on}) of approximately 0.5 V under forward bias (which indicates that the device will have fairly low power consumption), in line with the one reported for a ZnO NR array/p-Si based diode by Badran et al. (V_{on}=0.5 V) [39]. On the other hand, this turn-on voltage value is better than the one reported for a similar diode structure by Klason et al. (V_{on}=1.0 V) [19]. In both literature cited cases, the ZnO nanorod arrays have been grown onto the p-type silicon substrate [19,39]. Moreover, the junction shows an excellent diode rectifying behavior: the rectification ratio of the forward-to-reverse bias current is ca. 4.8×10^3 and 2.5×10^4 at a voltage of ±2 V and ±10 V, respectively. This rectification ratio value is

comparable with the value of 2.26×10^3 (at ±3 V) reported by Hwang et al. [15] for an heterojunction structure of ZnO nanorods/p-Si (where the ZnO nanorods have been grown by a hydrothermal method onto an annealed hydrothermal grown ZnO seed layer onto a silicon substrate); and much higher than the results of 6.3 (at ±2 V) [39] and 2.5×10^3 (at ±4 V) [24] reported in the literature, for ZnO NRs/p-Si heterostructures where the ZnO nanorods have been grown onto the p-silicon substrate via thermal evaporation of metallic zinc powder in the presence of oxygen and hydrothermal method, respectively. This very good rectification ratio value can be due to the good quality of ZnO nanorods and good interface characteristics of the device [24]. Moreover, such high value of rectification ratio can be attributed to the fact that the well-aligned ZnO NR arrays display good transport properties consisting of high electron mobility and provide the electrons with a direct electrical pathway [17]. The leakage current is only 4.5×10^{-7} A at a reverse bias of 10 V, which is in accordance with the reported value of 5.58×10^{-7} A for a ZnO nanowire array/p-Si heterojunction diode in which the ZnO nanowires have been grown onto the p-Si substrate by a hydrothermal method [40]. Such a low leakage current value suggests that there are few leakage pathways in the device, verifying also the formation of intimate ZnO/p^+-Si interface [17].

The diode-like behavior of the ZnO nanorod array/p^+-Si (100) heterojunction contact diode device was examined using thermionic emission model [16,41]. According to this model, the junction under forward bias has the I-V relation as:

$$I = I_S\left[\exp\left(\frac{qV}{nkT}\right) - 1\right] \qquad (V \geq 3k_BT/q), \qquad (1)$$

where V is the applied bias voltage (in V), I is the measured current, I_S is the saturation current, q is the absolute value of the electronic charge (in C), k and T are Boltzmann's

constant and absolute temperature, respectively, n is the ideality factor (in the ideal case n=1, if the transport mechanism is not governed exclusively by a thermionic emission process, n>1). The saturation current I_S is expressed as:

$$I_S = AA^*T^2 \exp\left(-\frac{q\Phi_b}{kT}\right) \qquad (2)$$

where A is the junction area, A* is the effective Richardson constant and Φ_b is the barrier height at the ZnO/ p^+-Si interface. The slope and the intercept from the linear fit to the semilog plot of the I-V curve depicted in Fig. 3c yield the ideality factor, n=2.8, and the barrier height, Φ_b=0.85 eV. A value greater than 2 for n indicates that the diode is not an ideal one. This is probably due to the presence of surface states and/or the presence of an insulating interfacial oxide layer (SiO_2) [11,42]. However, this obtained ideality factor value is lower than other ones reported in the literature for similar ZnO NR array/p-Si based diode devices, i.e. n=12.36 [40] and n=3.91 [19]. The calculated barrier height (Φ_b=0.85 eV), is rather close to previous reported values of 0.77 eV [19] and 0.82 eV [11]. Moreover, this calculated barrier height is in agreement to the difference of the work functions of Si (ca. 4.97-5.15 eV as it is heavily doped) and ZnO (4.25 eV) [11], i.e., 0.72-0.90 eV. Figure 4 shows an energy band diagram based on published data for the involved materials [4,43,44].

In order to determine the charge transport mechanism of the ZnO nanorod array/p^+-Si (100) heterojunction contact diode device, its I-V characteristic is presented in log-log scale in Fig. 5. The forward bias log I-log V curve is characterized by distinct linear regions (depending on the junction voltage value), indicating different conduction mechanisms [22,45]. As can be seen in Fig. 5, the forward bias characteristics show three linear regions separated by transition segments. At very low forward voltage for V

< 0.1 V (region I, slope 1.2), a linear dependence of the current on the voltage (I~V) is observed which indicates a transport mechanism obeying the Ohmic law. This small deviation from the ohmic behavior (slope 1.2 and not 1.0), indicates that the transport mechanism is most likely depending on the nature of contacts and on the presence of surface states and/or on the presence of an inherent insulating SiO_2 thin layer at the interface ZnO NR/p^+-Si(100) [46]. At higher voltage level, for 0.1 V<V< 0.4 V, (region II), the slope is measured to be 3.4. In this region, the current exponentially increases following the equation I~exp(αV), where α is a constant [22,46]. Aksoy et al. reported similar results [22]. This current behavior is often observed in the wide band gap p-n diodes [22,46]. At a moderately higher junction voltage, 0.4 V< V< 10 V, (region III, slope 2.3), the I-V characteristic follows a power law $I \sim V^{2.3}$. An exponent greater than 2 is indicative of space-charge-limited current [22,45]. Similar results have been reported in the literature [22,45].

4. CONCLUSIONS

A ZnO nanorod array/p-Si vertical heterojunction diode, in which the ZnO nanorods have been grown by electrodeposition onto a FTO/glass substrate, has been fabricated by the direct-bonding technique. Single-crystalline wurtzite structure of ZnO nanorods with a preferential growth along *c*-axis has been verified by microstructural studies. The heterojunction diode device showed a very good rectifying behavior with a rectification ratio of the forward-to-reverse bias current as ca. 4.8×10^3 and 2.5×10^4 at a voltage of ±2 V and ±10 V, respectively. The I-V characteristic was examined in the framework of the thermionic emission model. The obtained ideality factor and the barrier height values of the diode are 2.8 and 0.85 eV, respectively. The conduction mechanisms have been investigated from I-V characteristics as well. In summary, a simple, low cost and low

temperature process has been provided for the fabrication of ZnO nanorod array/p^+-Si vertical heterojunction diodes, which opens up significant opportunities for the production of photonic and electronic nanodevice arrays.

Acknowledgements.

The authors are grateful to MINECO of Spain, for the financial support received (Consolider Ingenio 2010 FUNCOAT-CSD2008-00023 & TEC2010-16700). This work was partially supported by CSIC (Comisión Sectorial de Investigación Científica) of the Universidad de la República, in Montevideo, Uruguay, and PEDECIBA – Física. R.S. thanks the support received by the D.I.-Pontificia Universidad Católica de Valparaíso, Valparaíso, Chile.

REFERENCES

[1] T. Pauporté, Toward Functional Nanomaterials, Lecture Notes in Nanoscale Science and Technology 5 (2009) 77-125.

[2] D.J. Rogers, F. H. Teherani, A. Yasan, K. Minder, P. Kung, M. Razeghi, Appl. Phys. Lett. 88 (2006) 141918.

[3] T. P. Chen, S. J. Young, S. J. Chang, C. H. Hsiao, C. S. Huang, J. Electrochem. Soc. 159 (2012) J153.

[4] M. Willander *et al,* Nanotechnology 20 (2009) 332001.

[5] J. Chung, J. Myoung, J. Oh, S. Lim, J. Phys. Chem. C 114 (2010) 21360.

[6] G. Guerguerian, F. Elhordoy, C. J. Pereyra, R. E. Marotti, F. Martín, D. Leinen, J. R. Ramos-Barrado, E. A. Dalchiele, Nanotechnology 22 (2011) 505401.

[7] G. Guerguerian, F. Elhordoy, C.J. Pereyra, R.E. Marotti, F. Martín, D. Leinen, J. R. Ramos-Barrado, E. A. Dalchiele, J. Phys. D: Appl. Phys. 45 (2012) 245301.

[8] C.D. Bojorge, V.R. Kent, E. Teliz, H.R. Canepa, R. Henríquez, H. Gómez, R.E. Marotti, E.A. Dalchiele, Phys. Status Solidi A 208 (2011) 1662.

[9] V. Consonni, G. Rey, J. Bonaimé, N. Karst, B. Doisneau, H. Roussel, S. Renet, D. Bellet, Appl. Phys. Lett. 98 (2011) 111906.

[10] D.K. Hwang, M.S. Oh, J.H. Lim, S.J. Park, J. Phys. D: Appl. Phys. 40 (2007) R387.

[11] S. Mridha, D. Basak, J. Appl. Phys. 101 (2007) 083102.

[12] X. Mo, G. Fang, H. Long, S. Li, H. Huang, H. Wang, Y. Liu, X. Meng, Y. Zhang, C. Pan, J. Lumin. 137 (2013) 116.

[13] A. Baltakesmez, S. Tekmen, S. Tüzemen, J. Appl. Phys. 110 (2011) 054502.

[14] Zhang, H. Guo, Z. Feng, L. Lin, J. Zhou, Z Lin, Electrochim. Acta 55 (2010) 4889.

[15] J.D. Hwang, Y.H. Chen, Thin Solid Films 520 (2012) 5409.

[16] J. Rodríguez-Moreno, E. Navarrete-Astorga, F. Martín, R. Schrebler, J.R. Ramos-Barrado, E.A. Dalchiele, Thin Solid Films 525 (2012) 88.

[17] Z. Yuan, J. Yu, W. Ma, Y. Jiang, Appl. Phys. A 106 (2012) 511.

[18] M. Willander, O. Nur, S. Zaman, A. Zainelabdin, N. Bano, I. Hussain, J. Phys. D: Appl. Phys. 44 (2011) 224017.

[19] M. Willander, R. Turan, O. Nur, Q.H. Hu, M.M. Rahman, P. Klason, Microelectron. J. 40 (2009) 706.

[20] A. E. Rakhshani J. Appl. Phys. 108 (2010) 094502.

[21] V. Quemener , M. Alnes, L. Vines , P. Rauwel, O. Nilsen, H. Fjellvåg, E.V. Monakhov, B.G. Svensson, J. Phys. D: Appl. Phys. 45 (2012) 315101.

[22] S. Aksoy, Y. Caglar, Superlattices and Microstruct. 51 (2012) 613.

[23] M. Soylu, M. Girtan, F. Yakuphanoglu, Mater. Sci. Eng., B 177 (2012) 785–790.

[24] C.W. Cao, W.N. Bao, X. Lin, X.Y. Liu, Y. Geng, H.L. Lu, Q.Q. Sun, P. Zhou, D. Zhang, P.F. Wang, ECS Solid State Letters 2 (2013) Q25.

[25] Y. Xie, M. Madel, Y. Li, W. Jie,B. Neuschl, M. Feneberg,K. Thonke J. Appl. Phys. 112 (2012)123111.

[26] B. Jung, J.H. Lee, J.Y. Lee, J.H. Kim, H.K. Cho J. Electrochem. Soc. 159 (2012) H102.

[27] S.W. Lee, H.D. Cho, G. Panin, T.W. Kang, Appl. Phys. Lett. 98 (2011) 093110.

[28] H.Y. Yang, S.F. Yu, H.K. Liang, T.P. Chen, J. Gao, T. Wu, Opt Express 18 (2010) 15585.

[29] M. Izaki and T. Omi, J. Electrochem. Soc. 143 (1996) L53.

[30] S. Peulon and D. Lincot, Adv. Mater. 8 (1996) 166.

[31] D. Lincot, Thin Solid Films 487 (2005) 40.

[32] R.K. Pandey, S.N. Sahu and S. Chandra, Handbook of Semiconductor Electrodeposition (CRC Press, 1996), ISBN: 0824797019.

[33] G.W. She, X.H. Zhang, W.S. Shi, X. Fan, J.C. Chang, C.S. Lee, S.T. Lee, C.H. Liu, Appl. Phys. Lett. 92 (2008) 053111.

[34] O. Lupan, T. Pauporté, I.M. Tiginyanu, V.V. Ursaki, H. Heinrich, L. Chow, Mater. Sci. Eng. B 176 (2011) 1277.

[35] M.R. Khajavi, D.J. Blackwood, G. Cabanero, R. Tena-Zaera, Electrochim. Acta 69 (2012) 181.

[36] S. M. Sze, In Semiconductor devices, physics and technology (Wiley, New York, 1985).

[37] M. J. Sailor Porous Silicon in Practice: Preparation, Characterization and Applications (Weinheim, Germany: Wiley-VCH Verlag & Co. KGaA, 2012).

[38] Powder Diffraction File, Joint Committee for Powder Diffraction Studies (JCPDS) File No. 05-0664 (hexagonal structure of ZnO).

[39] R.I. Badran, A. Umar, S. Al-Heniti, A. Al-Hajry, T. Al-Harbi, J. Alloys Compd. 508 (2010) 375–379.

[40] D. Shao, M. Yu, J. Lian, S. Sawyer, Appl. Phys. Lett. 101 (2012) 211103.

[41] Sze S M, in Semiconductor Devices, 2nd ed. Wiley, New York, 2001, p. 224.

[42] Y. Caglara, M. Caglara, S. Ilicana, F. Yakuphanoglub, Microelectron. Eng. 86 (2009) 2072.

[43] R.C. Chiechi, E.A. Weiss, M.D. Dickey, G.M. Whitesides, Angew. Chem. Int. Ed. 47 (2008) 142.

[44] M.G. Helander, M.T. Greiner, Z.B. Wang, W.M. Tang, J. Vac. Sci. Technol. A 29 (2011) 011019.

[45] R. Ghosh, D. Basak, Appl. Phys. Lett. 90(2007) 243106.

[46] N. Zebbar,Y. Kheireddine, K. Mokeddem, A. Hafdallah, M. Kechouanea, M. S. Aida, Mater. Sci. Semicond. Process. 14 (2011) 229.

FIGURE CAPTIONS.

Figure 1. (a) Tilted FE-SEM micrograph view with a tilt angle of 50^{o} of a typical ZnO nanorod array electrochemically grown onto a FTO substrate. The inset shows a high magnification image of a single vertical free standing ZnO nanorod, revealing its hexagonal prism shape with planar top ends. (b) TEM image of a single ZnO nanorod mechanically detached from the ZnO nanorod array/FTO glass substrate. (c) HRTEM micrograph of a single ZnO nanorod, the inset (d) shows the corresponding SAED pattern, indicating the single-crystalline characteristic of the nanorod.

Figure 2. X-ray diffraction pattern of a ZnO nanorod array sample. Diffraction planes are indicated for ZnO. Hexagonal wurtzite ZnO JCPDS pattern is also shown for comparison (ZnO JCPDS: thick blue bars). (*, indicates the peaks originated from the SnO_2:F substrate).

Figure 3. (a) Cross-sectional schematic diagram of the vertical ZnO nanorod array/p^{+}-Si (100) heterojunction contact diode device. (b) I-V characteristics of FTO contact on ZnO nanorod array (continuous black line), and FTO glass substrate/p^{+}-Si(100) device (as depicted in (a) but without the presence of ZnO NRs) (dashed red line). Inset : I-V curves on a semi-log scale showing symmetric electrical behavior. (c) Current-voltage (I-V) characteristics of a typical vertical ZnO nanorod array/p^{+}-Si (100) heterojunction contact diode device in a linear and a semi-log form.

Figure 4. Energy band diagram for the ZnO nanorod array/p^{+}-Si (100) heterojunction contact diode device with work function values for the contact, and conduction and valence band edges for ZnO and Si.

Figure 5. Log-Log plot of the current-voltage under forward bias of ZnO nanorod array/p^+-Si (100) heterojunction. The I-V plot is divided into three different regions. The dashed lines represent the theoretical fittings to the data, and the respective slope values are indicated as m_1, m_2 and m_3.

FIGURE 1.

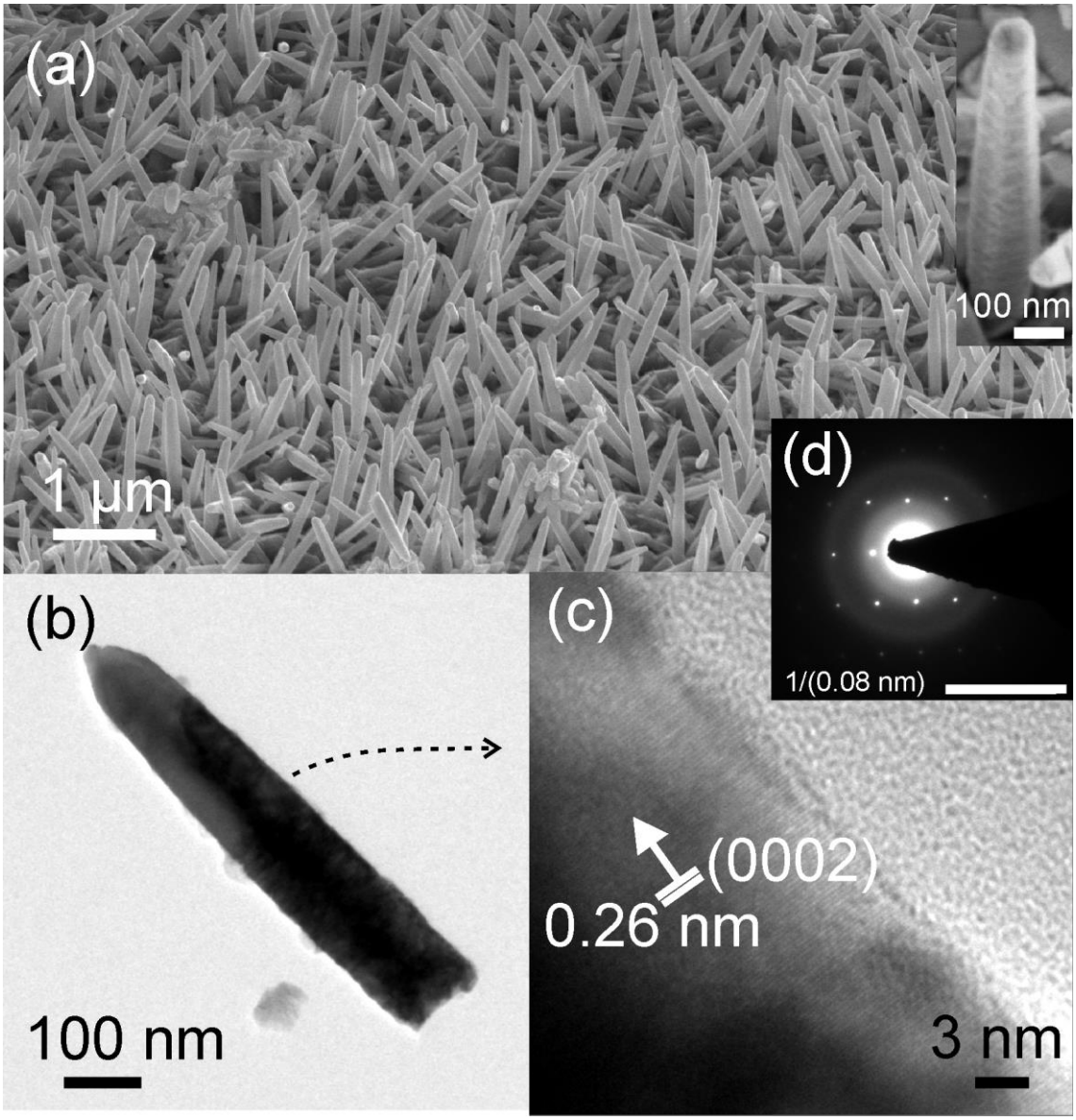

FIGURE 2.

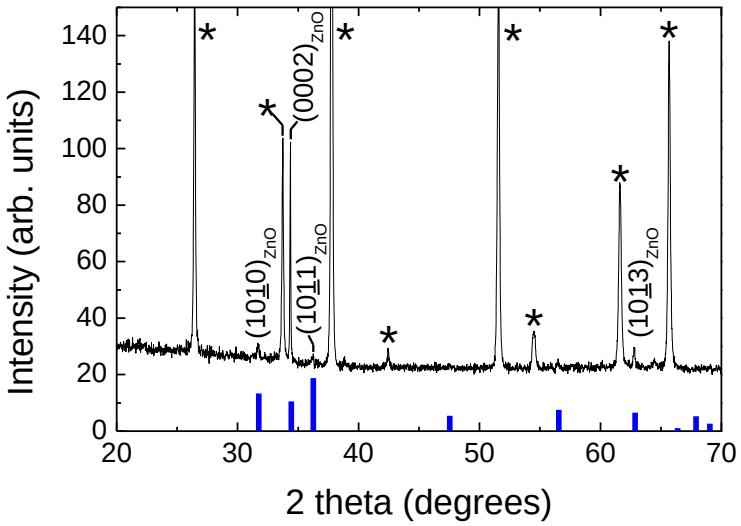
Intensity (arb. units)
2 theta (degrees)
(10$\bar{1}$0)$_{ZnO}$
(0002)$_{ZnO}$
(10$\bar{1}$1)$_{ZnO}$
(10$\bar{1}$3)$_{ZnO}$

FIGURE 3.

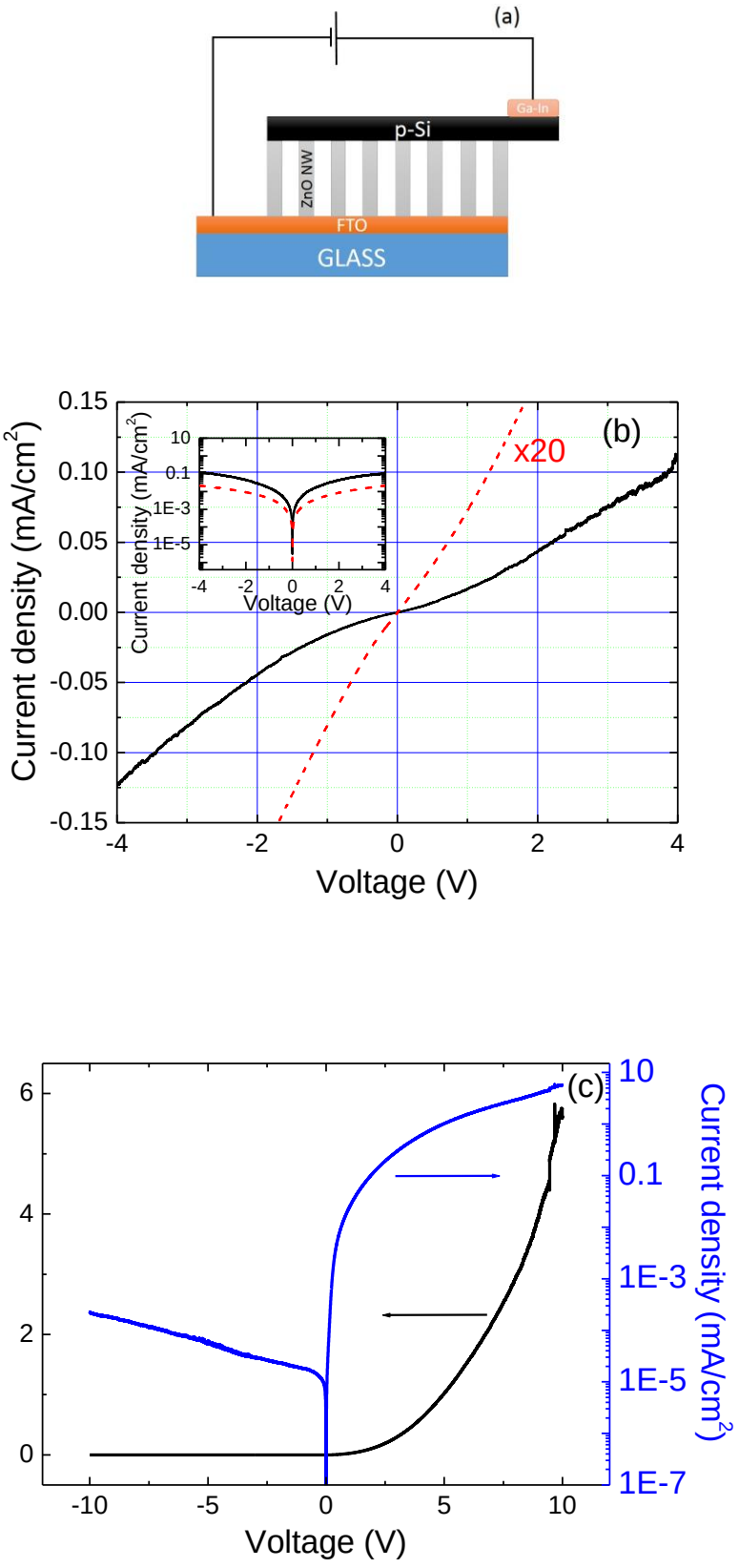
(a)
Ga-In
p-Si
ZnO NW
FTO
GLASS
(b)
x20
Current density (mA/cm^2)
Voltage (V)
0.15
0.10
0.05
0.00
-0.05
-0.10
-0.15
-4
-2
0
2
4
10
0.1
1E-3
1E-5
(c)
Current density (mA/cm^2)
Current density (mA/cm^2)
Voltage (V)
6
4
2
0
-10
-5
0
5
10
10
0.1
1E-3
1E-5
1E-7

FIGURE 4.

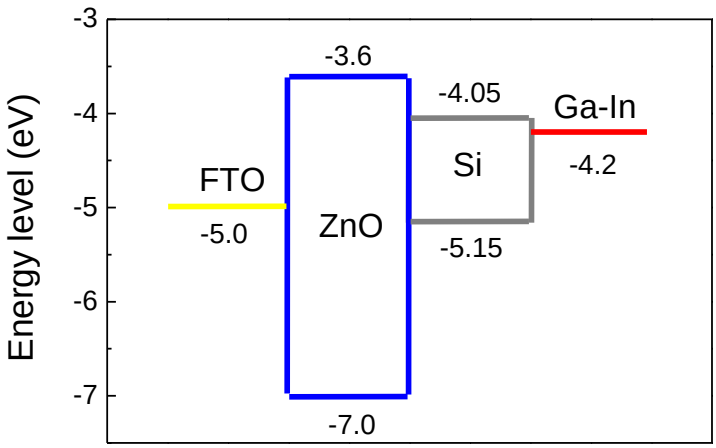

FIGURE 5.

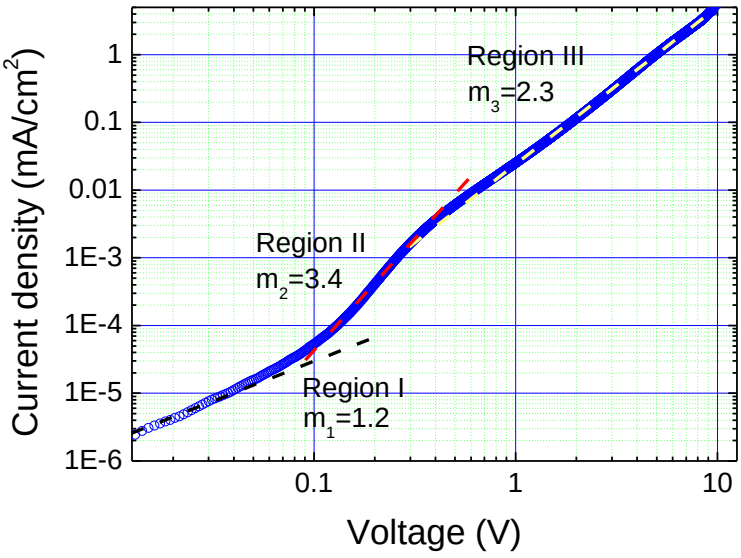
Current density (mA/cm^2)
1
0.1
0.01
1E-3
1E-4
1E-5
1E-6
0.1
1
10
Voltage (V)
Region III
m_3=2.3
Region II
m_2=3.4
Region I
m_1=1.2